Biophysical Journal, Volume *122*

Supplemental information

Predicting YAP/TAZ nuclear translocation in response to ECM mechanosensing

Bo Cheng, Moxiao Li, Wanting Wan, Hui Guo, Guy M. Genin, Min Lin, and Feng Xu

Supplementary Materials for "Predicting YAP/TAZ Nuclear Translocation in Response to ECM Mechanosensing"

Bo Cheng[1,2], Moxiao Li[3#], Wanting Wan[2,4], Hui Guo[5], Guy M. Genin[1,2,6], Min Lin[1,2], Feng Xu[1,2#]

[1] *MOE Key Laboratory of Biomedical Information Engineering, School of Life Science and Technology, Xi'an Jiaotong University, Xi'an 710049, P.R. China*

[2] *Bioinspired Engineering and Biomechanics Center (BEBC), Xi'an Jiaotong University, Xi'an 710049, P.R. China*

[3] *State Key Laboratory of Mechanics and Control of Mechanical Structures, Nanjing University of Aeronautics and Astronautics, Nanjing 210016, China*

[4] *Key Laboratory of Shaanxi Province for Craniofacial Precision Medicine Research, College of Stomatology, Xi'an Jiaotong University, Xi'an 710004, P.R. China*

[5] *Department of Medical Oncology, The First Affiliated Hospital of Xi'an Jiaotong University, Xi'an 710004, P.R. China*

[6] *NSF Science and Technology Center for Engineering Mechanobiology, Washington University in St. Louis, St. Louis 63130, MO, USA*

[#] *Corresponding authors:* moxiaoli@nuaa.edu.cn, fengxu@mail.xjtu.edu.cn

Contents:

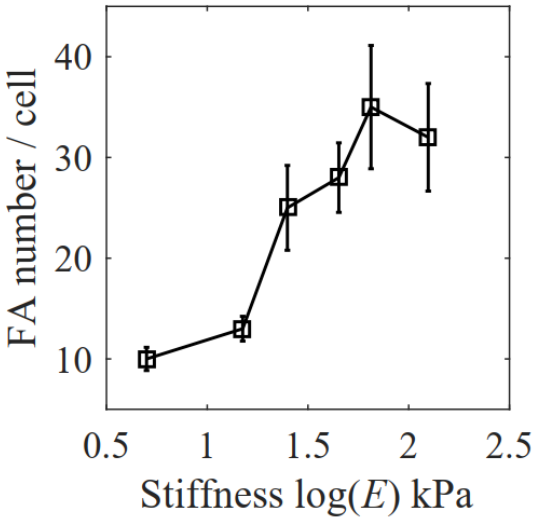

Figure S1. Effects of the stiffness of elastic matrix on the FA number.

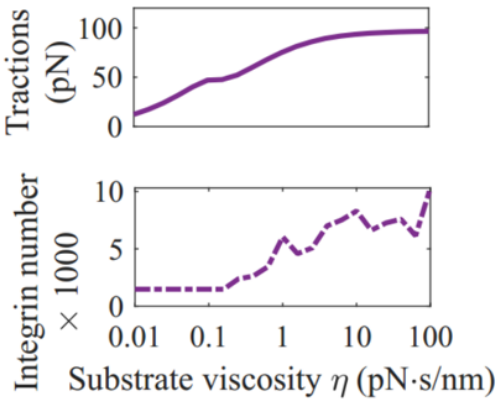

Figure S2. Cell traction and active integrin number both increase with matrix viscosity.

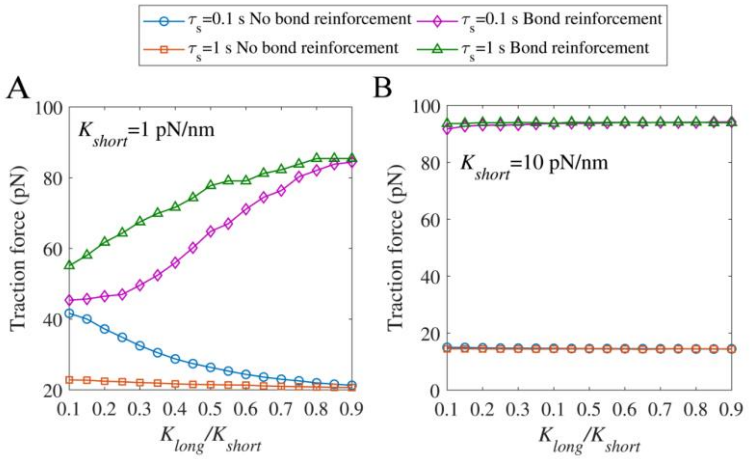

Figure S3. Effects of short-term stiffness of the viscoplastic substrate on cell traction force.

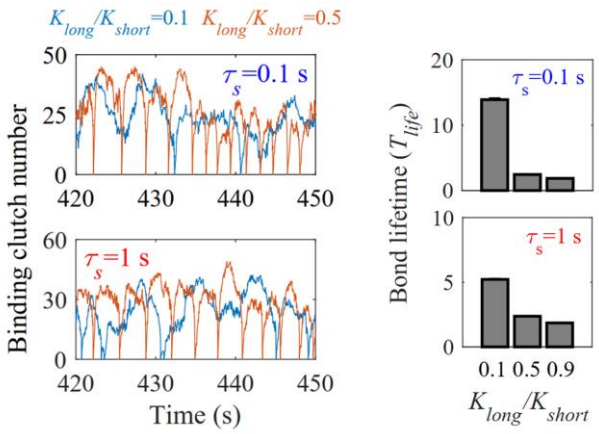

Figure S4. Lifetimes of bonds decrease with increasing K_{long}/K_{short} at different relaxation times (τ_s = 0.1 and 1 s).

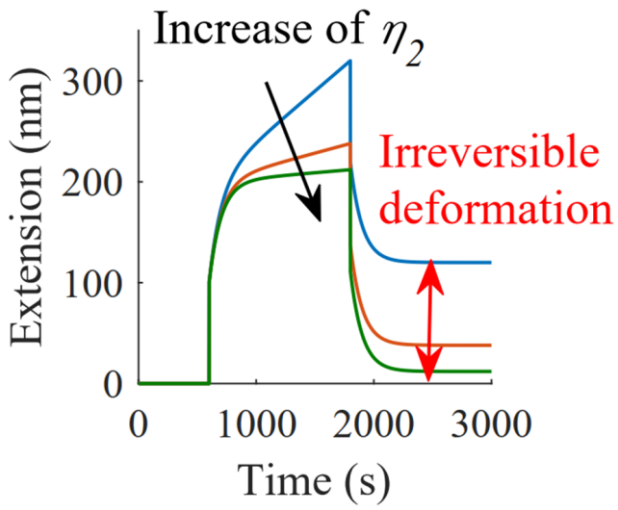

Figure S5. The mechanical parameter, η_2, represents the level of irreversible deformation of the matrix.

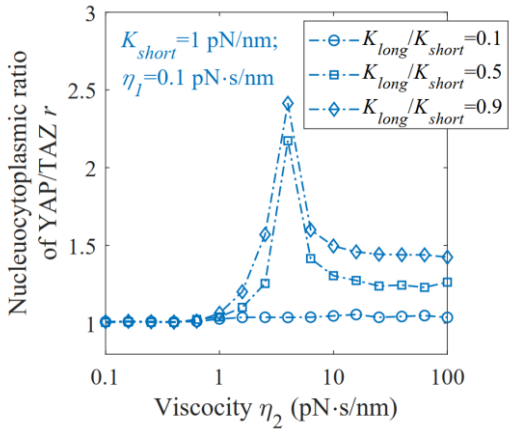

Figure S6. When the short-term stiffness is relatively small, the YAP/TAZ ratio first increases and then decreases with increasing η_2.

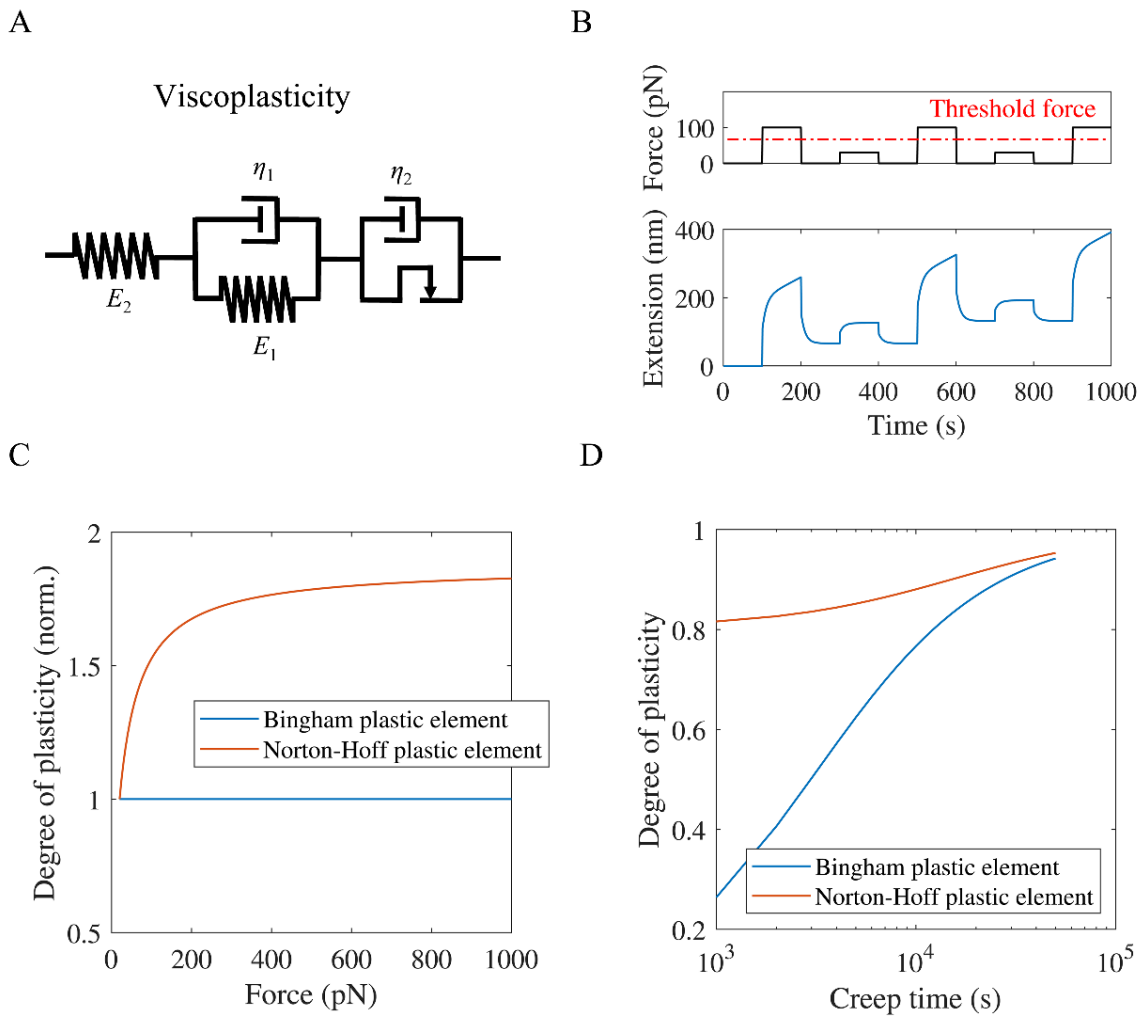

Figure S7. The threshold force and creep time can regulate the degree of plasticity of the matrix.

Supplementary Note 1 - Computational screening of mechanotherapeutics

To apply the computational model in the context of mechanomedicine, we performed computer simulations of how integrin-FAK-myosin-YAP/TAZ pathway inhibitors can control cellular sensing of matrix elasticity. To identify target inhibitors (*e.g.*, targeting integrin binding activity, myosin activation), we performed a sensitivity analysis on the entire suite of model parameters, and then identified inhibitors that affect the biochemical reactions (**Fig. S8**). The sensitivity analyses quantified how model parameters affect mechanosensitivity by evaluating how, for each set of parameters, the YAP/TAZ N/C ratio (r) would vary with matrix stiffness (E) in the Hill-type scaling law: $r = \frac{AE^2}{M+E^2} + B,$ where the Hill coefficient M describes the sensitivity range, B describes the response on a compliant matrix, and A describes the response on a stiff matrix (**Fig. S9**). The parameters fell into three categories: (*i*) adhesion dynamics parameters, including retrograde flow rate (V_0), integrin stiffness (K_{link}), integrin density (N_{link}), myosin stall force (F_{stall}), talin unfolding force (F_{unfold}), adhesion reinforcement rate (d_{add}), adhesion reinforcement threshold force (F_{cr}), integrin binding and unbinding rates (k_{on}^0, k_{off}^0) and clutch bond characteristic rupture force (F_{b}); (*ii*) cytoplasmic signaling dynamics parameters, including auto-phosphorylation and dephosphorylation rates of FAKY397 ($k_{\text{FAK-a}}$, $k_{\text{FAK-ina}}$), activation and deactivation of ROCK ($k_{\text{ROCK-a}}$, $k_{\text{ROCK-ina}}$), mDia ($k_{\text{mDia-a}}$, $k_{\text{mDia-ina}}$), myosin ($k_{\text{myosin-a}}$, $k_{\text{myosin-ina}}$), and F-actin polymerization ($k_{\text{F-actin-a}}$) and depolymerization ($k_{\text{F-actin-ina}}$); (*iii*) nucleocytoplasmic shuttling dynamics parameters including the stiffnesses of FG and YAP (K_{FG}, K_{YAP}), YAP/TAZ nuclear import and export rates (k_{YAPin}, k_{YAPout}), and the YAP unfolding force ($F_{\text{YAP-unfold}}$). The Hill-type function is used to fit the simulation results. We found that talin unfolding force, nuclear deformation coefficients and FAK activation rates influence the Hill coefficient (K) and thus the stiffness range for mechanosensing (**Fig. S9**). Integrin density, nuclear deformation coefficients, and activation and deactivation rates of FAK and ROCK are found to influence α, and thus the response on stiff matrices.

Method for parameter sensitivity analysis

The sensitivity value S of the level of nucleocytoplasmic ratio of YAP/TAZ to a parameter p is defined as: $S = \frac{d\log(r)}{d\log(p)},$ where p is the base parameter value, and r is the nucleocytoplasmic ratio of YAP/TAZ at the base parameter value. The S value is equivalent to the slope of r versus p on a log-log plot and represents the fold-change in the nucleocytoplasmic ratio of

YAP/TAZ resulting from a fold-change in a parameter value (0.1-, 1- and 10-fold changes of the base parameter). A line was fitted to the data points with the slope of the line taken to be the *S* value.

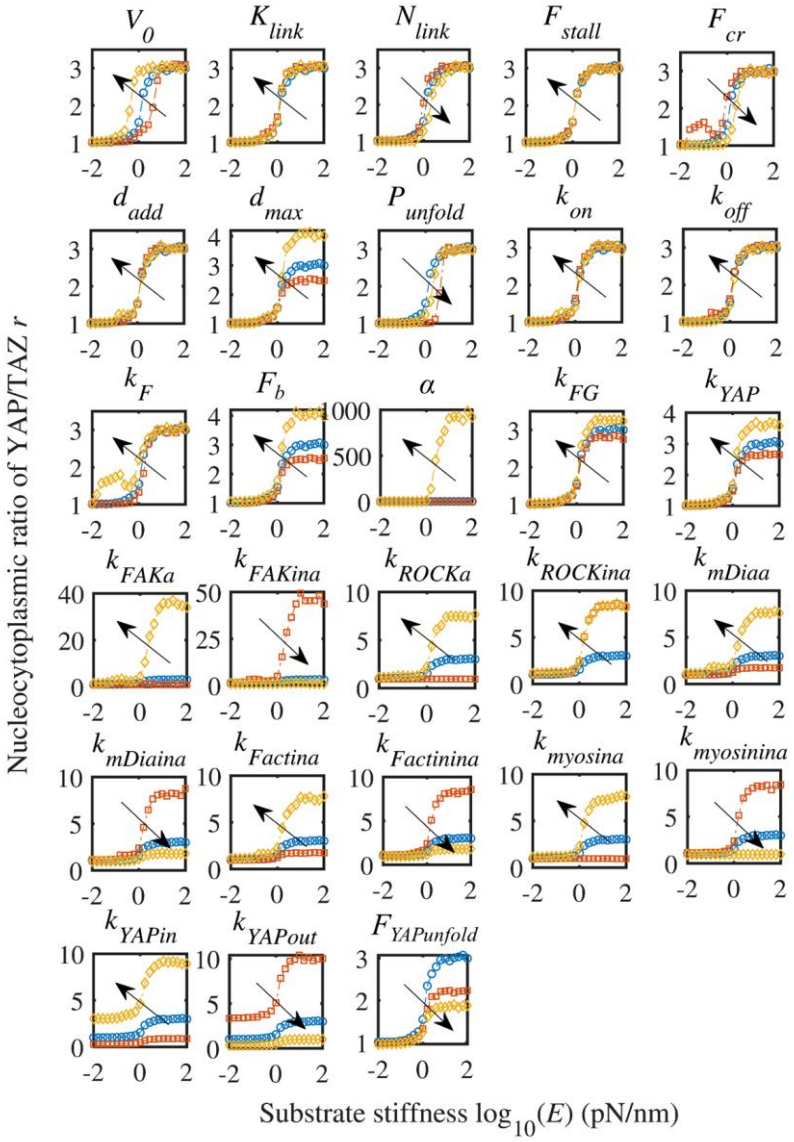

Figure S8. Parameter sensitivity analysis of cell adhesion, signaling and nucleocytoplasmic shuttling dynamics of YAP/TAZ in the integrated model for the elastic substrate.

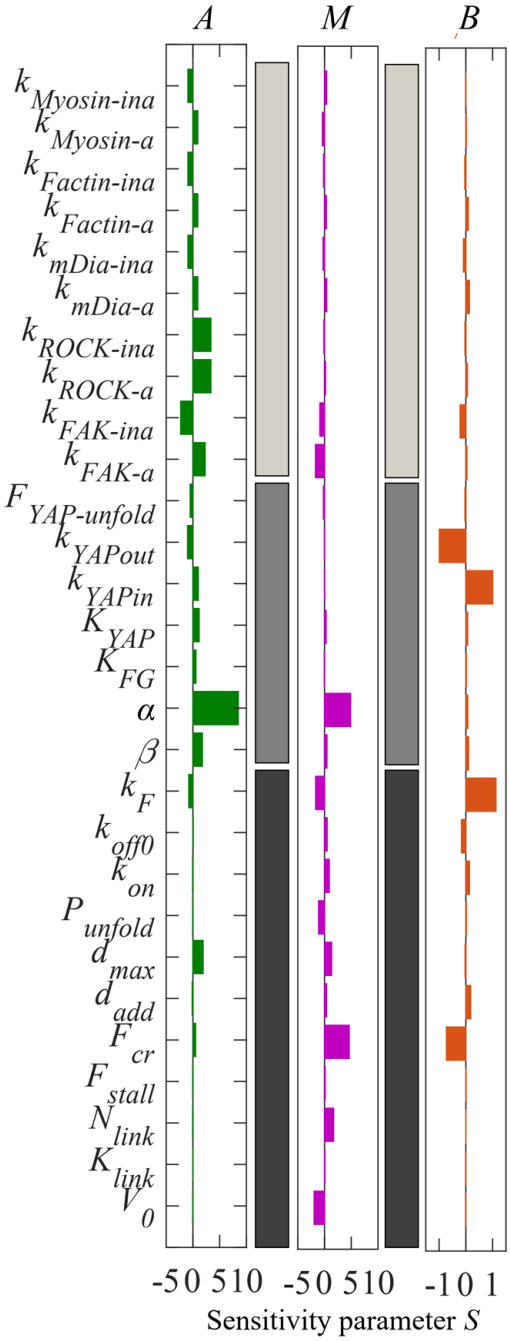

Figure S9. Parameter sensitivity analysis about adhesion dynamics, signal transduction and nuclear deformation dynamics.

Supplementary Note 2 - Model parameters

- *Parameters for integrin-clutch dynamics (**Table S1**)*

F_{stall} is the stall force of motor where the rate of actin flow is equal to zero, *i.e.*, $F_{stall} = n_m F_m$, where F_m is the maximum force that each single motor can exert and the n_m is the myosin number. Molloy *et al*. showed that a single myosin head can produce a force of ~1-2 pN under isometric conditions (1). In our model, F_m = 2 pN. As for n_m, we set the same value as in the literature (2), *i.e.*, n_m = 50, in order to ensure that the maximal adhesion force is within a range of quantities, ~100 pN as measured in (3).

V_0 is the maximum actin flow rate which is also the unloaded myosin motor velocity. Elosegui-Artola *et al.* (4) and Chan *et al.* (3) have measured that actin flow rates with the minimal integrin bond connection are ~100-120 nm/s.

N_{link} is the number of clutch bonds. This is a free parameter that is set to slow retrograde flow to experimentally observed level ranging between 120 pN/nm and 40 pN/nm (4). Usually, for motor-clutch system, we set the number of clutch bonds and the number of motors to be equal in simulations to ensure cells can perform effective stiffness-sensing (2).

F_b is the characteristic rupture force of substrate-actin clutch bond. Jiang *et al*. showed that such rupture force of slip bond is ~2 pN (5).

k_{on}^0 is the true binding rate of integrins. Elosegui-Artola *et al*. have experimentally shown that the true binding rates of $\alpha_5\beta_1$-FN and $\alpha_v\beta_6$-FN bonds are 6.1×10^{-5} $\mu m^2/s$ and 6×10^{-5} $\mu m^2/s$, respectively (4). Besides, Litvinov et al. showed that $\alpha_{II}\beta_3$-fibrinogen binding rate is $1\text{-}2\times10^{-4}$ $\mu m^2/s$. Since $\alpha_5\beta_1$ integrins are the main type of mechanosensing molecule, we set true binding rate to be 6×10^{-5} $\mu m^2/s$.

k_{off}^0 is the bond off-rate. This is the pseudo first-order unloaded off-rate constant for clutch dissociation from F-actin. Lele et al. showed that the range of values for bond off-rate is 0.01-0.1 s^{-1} (7).

K_{link} is the motor-clutch spring constant. Roca-Cusachs *et al*. showed that the stiffness of talin is ~1.5 pN/nm and of FN is ~0.5 pN/nm (8). Since the unfolding and reinforcement processes

of clutch bonds occur mainly on talin molecules, we set this value to be 0.8 pN/nm.

d_{int} is the integrin density on the membrane and d_{add} is the added integrin density during the reinforcement process. Note that as described in (4), d_{add} does not influence the results of motor-clutch dynamics, which just regulates the time required by the simulation to reach steady state. So we set d_{add} = 4/μm^2 (4). Integrin densities on the membrane is measured experimentally ~488/μm^2 for $\alpha_5\beta_1$ and ~2513/μm^2 for $\alpha_v\beta_6$ (4). Considering that the $\alpha_5\beta_1$ integrins are the main type of mechanosensing molecule, we set this value to be 500/μm^2.

F_{cr} is the threshold force for adhesion reinforcement. When $F_s > F_{cr}$, the density of integrins increases with a value of d_{add}. Here, in our model, we set F_{cr} = 87 pN which is consistent with (4).

P_a is the radius of the circular adhesion site. It has been shown that the typical length scale of cell adhesions is on the order of ~1-2 μm (9). Thus, we set P_a = 550 nm, which is also consistent with (4).

Table S1. Baseline of model parameters for integrin-clutch and substrate mechanics

Parameter	Symbol	Value	Refs
Stall force of motor	F_{stall}	100 pN	(1)
Maximum actin flow rate	V_0	120 nm/s	(2)
Number of clutch bonds	N_{link}	50	(2)
Characteristic rupture force of clutch bond	F_b	2 pN	(5)
Bond on-rate	k_{on}^0	6×10^{-5} μm^2 s^{-1}	(4)
Bond off-rate	k_{off}^0	0.1 s^{-1}	(7)
Bond spring constant	K_{link}	0.8 pN/nm	(8)
Threshold force for adhesion reinforcement	F_{cr}	87 pN	(4)
Added integrin density	d_{add}	4 μm^{-2}	(4)
Integrin density on the membrane	d_{int}	500 μm^{-2}	(4)
Radius of circular adhesion site	P_a	550 nm	(4)
Stiffness for elastic substrate	E	10^{-2}~10^2 pN/nm	adjust

Long-term stiffness for viscoelastic substrate	E_l	10^{-2}~10^{2} pN/nm	adjust
Additional stiffness for viscoelastic substrate	E_a	10^{-2}~10^{2} pN/nm	adjust
Viscosity for viscous substrate	η	10^{-2}~10^{2} pN·s/nm	adjust

- *Parameters for intracellular signaling pathways*

Parameters of the intracellular signaling pathway are obtained and supported from the existing literature (**Table S2**).

Table S2. Baseline of model parameters for intracellular signaling pathway

Parameter	Symbol	Value	Refs
Auto-phosphorylation rate of FAK	$k_{\text{FAK-a}}$	0.015 s^{-1}	(10) (11)
Dephosphorylation rate of FAK	$k_{\text{FAK-ina}}$	0.035 s^{-1}	(11) (12)
Activation rate of RhoA	$k_{\text{Rho-a}}$	0.0168 s^{-1}	(11)
Deactivation rate of RhoA	$k_{\text{Rho-ina}}$	0.625 s^{-1}	(11) (13)
Activation rate of ROCK	$k_{\text{ROCK-a}}$	2.2 s^{-1}	(10) (14)
Deactivation rate of ROCK	$k_{\text{ROCK-ina}}$	0.8 s^{-1}	(10) (15)
Activation rate of mDia	$k_{\text{mDia-a}}$	1 s^{-1}	(10) (16)
Deactivation rate of mDia	$k_{\text{mDia-ina}}$	1 s^{-1}	(10) (11)
Activation rate of myosin	$k_{\text{myosin-a}}$	0.03 s^{-1}	(11)
Deactivation rate of myosin	$k_{\text{myosin-ina}}$	0.067 s^{-1}	(11)
F-actin polymerization rate	$k_{\text{F-actin-a}}$	0.4 s^{-1}	(17)
F-actin depolymerization rate	$k_{\text{F-actin-ina}}$	3.5 s^{-1}	(17)

- *Parameters for YAP/TAZ dynamics (**Table S3**)*

α is the nuclear pore deformation coefficient which is the intensity of nuclear stress's effect on nuclear pore deformation. Our previous study showed that the nuclear pore is linearly related to nuclear stress (18). Thus, for simplicity, we here assumed that perinuclear forces F also is proportional to nuclear stress, *i.e.*, $\alpha = 1$.

$k_{\text{YAP-in}}$ and $k_{\text{YAP-out}}$ are the YAP/TAZ nuclear import and export rate, respectively. $k_{\text{YAP-in}}$ is the rate of import of YAP/TAZ to nucleus due to the increased pore deformation. We can obtain

the import and export rates by fitting the FRAP experimental curves with an exponential function (19). Here, we set the import rate on a soft substrate (5 kPa) to be 0.1 s^{-1} and export rate on different substrates to be 0.3 s^{-1}.

$F_{YAP\text{-}unfold}$ is the YAP unfolding force. Elosegui-Artola *et al*. experimentally investigated the mechanical stability of YAP molecules by pulling single YAP molecule with an AFM (19). These results showed that, in the majority of the cases, YAP molecules can be unfolded at undetectable forces (<10 pN). Thus, we set YAP unfolding force to be 2 pN which is within an order of magnitude of the clutch unfolding force to ensure that cells have appropriate force-sensitive behavior.

About the stiffnesses of FG and YAP molecules. Bestembayeva *et al.* experimentally showed that the stiffness of FG-nup is ~1-5 pN/nm (20). As for YAP molecules, an estimated value obtained from the AFM data (19) (the example curves showing YAP/polyprotein extension as a function of forces) is used in the model. Thus, we set $K_{YAP} = K_{YAP} = \sim 2$ pN/nm.

Table S3. Baseline of model parameters for YAP/TAZ dynamics

Parameter	Symbol	Value	Refs
Nuclear pore deformation coefficients	α	1	adjust
Stiffnesses of FG	K_{FG}	2 pN/nm	(20)
Stiffnesses of YAP	K_{YAP}	2 pN/nm	Estimated from (19)
YAP/TAZ nuclear import rate	$k_{YAP\text{-}in}$	0.1 s^{-1}	Estimated from (19)
YAP/TAZ nuclear export rate	$k_{YAP\text{-}out}$	0.3 s^{-1}	Estimated from (19)
YAP unfolding force	$F_{YAP\text{-}unfold}$	2 pN	(19)

Supplementary Note 3 - Constitutive equations of SLS and Burgers model

- *The constitutive equations of standard linear viscoelastic solid (SLS):*

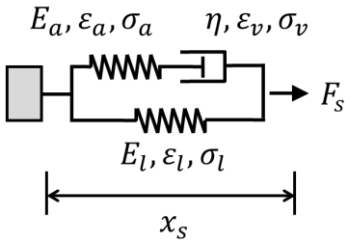

A force F_s acting on the standard linear viscoelastic solid, therefore,

$$F_s = \sigma_l + \sigma_a = \sigma_l + \sigma_v, \tag{S1}$$

$$x_s = \varepsilon_l = \varepsilon_a + \varepsilon_v. \tag{S2}$$

According to Hooke's law and Newton's law of flow,

$$\sigma_l = E_l \varepsilon_l = E_l x_s, \tag{S3}$$

$$\sigma_a = E_a \varepsilon_a, \tag{S4}$$

$$\sigma_v = \eta \dot{\varepsilon_v}. \tag{S5}$$

From Eq. S2,

$$\dot{x_s} = \dot{\varepsilon_a} + \dot{\varepsilon_v}. \tag{S6}$$

Substitute Eq. S4 and Eq. S5 into Eq. S6,

$$\dot{x_s} = \frac{\dot{\sigma_a}}{E_a} + \frac{\sigma_v}{\eta}. \tag{S7}$$

Substitute Eq. S1 into Eq. S7,

$$\dot{x_s} = \frac{\dot{F_s} - \dot{\sigma_l}}{E_a} + \frac{F_s - \sigma_l}{\eta}. \tag{S8}$$

Then,

$$\dot{x_s} = \frac{\dot{F_s} - E_l \dot{x_s}}{E_a} + \frac{F_s - E_l x_s}{\eta}. \tag{S9}$$

Then constitutive equations of standard linear viscoelastic solid as follows:

$$\eta(E_a + E_l)\dot{x_s} + E_a E_l x_s = \eta \dot{F_s} + E_a F_s. \tag{S10}$$

- *The constitutive equations of Burgers viscoplastic element:*

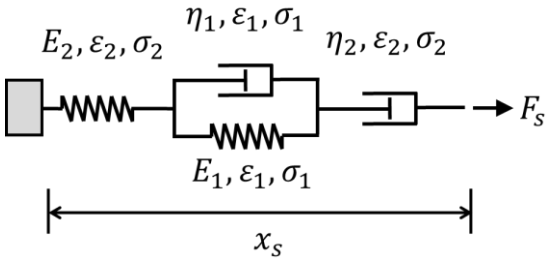

Let $D = \mathrm{d}/\mathrm{d}t$ stand for differential arithmetic and $V(D)$ represent the arithmetic polynomial. Now, there are two basic units $F_{s,1} = V_1(D)x_{s,1}$ and $F_{s,2} = V_2(D)x_{s,2}$. If the two units are "in series", then $F_s = F_{s,1} = F_{s,2}$ and $x_s = x_{s,1} + x_{s,2}$. The Burgers element is composed of Kelvin body and Maxwell body in series. Thus,

$$F_s = \frac{V_1(D)V_2(D)}{V_1(D) + V_2(D)} x_s, \tag{S11}$$

Then,

$$F_s = \frac{E_1E_2\eta_2 D + E_2\eta_1\eta_2 D^2}{E_1E_2 + (E_1\eta_2 + E_2\eta_1 + E_2\eta_2)D + \eta_1\eta_2 D^2} x_s, \tag{S12}$$

Then, we have

$$\eta_2\dot{x_s} + \frac{\eta_1\eta_2}{E_1}\ddot{x_s} = F_s + \left(\frac{\eta_1}{E_1} + \frac{\eta_2}{E_1} + \frac{\eta_2}{E_2}\right)\dot{F_s} + \frac{\eta_1\eta_2}{E_1E_2}\ddot{F_s}, \tag{S13}$$

Supplementary Note 4 - Coupling between substrate deformation and chemical reactions

First, the cell traction force in algorithm is calculated by:

$$F_s = \sum_{i=1}^{N_{link}} K_{link}\,(x_i - x_s) = K_{link} \sum_{i=1}^{N_{link}} x_i - x_s K_{link} N_{link} = F_{sum} - x_s K_{sum}. \tag{S14}$$

where F_{sum} is the sum of all closed bond deformation and K_{sum} is the sum of all closed bond stiffnesses; F_s is the force acting on the substrate and x_s is thus the strain of substrate. Later, the constitutive equations of substrates are discretized using a Backward Euler method and the cell traction force is calculated based on the new deformation of substrate. Details about method of substrate strain in algorithm are as follows:

For elastic model:

$$F_s = E x_s = F_{sum} - x_s K_{sum}, \tag{S15}$$

Then,

$$x_s = \frac{F_{sum}}{E + K_{sum}}. \tag{S16}$$

For viscous model:

$$F_s = \eta \dot{x_s} = F_{sum} - x_s K_{sum}, \tag{S17}$$

Then, we developed discrete format of differential equations by substituting,

$$\dot{x_{s,n+1}} = \left(x_{s,n+1} - x_{s,n}\right)/dt, \tag{S18}$$

$$F_{s,n+1} = F_{sum,n+1} - x_{s,n+1} K_{sum,n+1}. \tag{S19}$$

Then,

$$x_{s,n+1} = \frac{x_n}{A} + \frac{1}{A}\frac{dt}{\eta} F_{sum,n+1}, \tag{S20}$$

$$A = 1 + \frac{dt K_{sum,n+1}}{\eta}. \tag{S21}$$

For viscoelastic model:

First, we developed discrete format of differential equations by substituting,

$$\dot{x_{s,n+1}} = \left(x_{s,n+1} - x_{s,n}\right)/dt, \tag{S22}$$

$$\dot{F_{s,n+1}} = \left(F_{s,n+1} - F_{s,n}\right)/dt, \tag{S23}$$

$$F_{s,n+1} = F_{sum,n+1} - x_{s,n+1} K_{sum,n+1}, \tag{S24}$$

$$F_{s,n} = F_{sum,n} - x_{s,n}K_{sum,n}, \tag{S25}$$

$$(E_a + E_l)\eta\dot{x}_{s,n+1} + E_aE_lx_{s,n+1} = E_aF_{s,n+1} + \eta\dot{F}_{s,n+1}. \tag{S26}$$

Then,

$$x_{s,n+1} = \frac{A}{C}x_n + \frac{B}{C}, \tag{S27}$$

$$A = \frac{p_1K_{sum,n} + q_1}{dt}, \tag{S28}$$

$$B = \left(1 + \frac{p_1}{dt}\right)F_{sum,n+1} - \frac{p_1}{dt}F_{sum,n}, \tag{S29}$$

$$C = q_0 + \frac{q_1}{dt}K_{sum,n+1} + K_{sum,n+1}\frac{p_1}{dt}, \tag{S30}$$

$$p_1 = \frac{\eta}{E_a}, q_0 = E_l, q_1 = \frac{(E_a + E_l)\eta}{E_a}. \tag{S31}$$

For viscoplastic model:

First, we developed discrete format of differential equations by substituting,

$$\dot{x}_{s,n+1} = \left(x_{s,n+1} - x_{s,n}\right)/dt, \tag{S32}$$

$$\ddot{x}_{s,n+1} = \left(x_{s,n+1} - 2x_{s,n} + x_{s,n-1}\right)/dt^2, \tag{S33}$$

$$\dot{F}_{s,n+1} = \left(F_{s,n+1} - F_{s,n}\right)/dt, \tag{S34}$$

$$\ddot{F}_{s,n+1} = \left(F_{s,n+1} - 2F_{s,n} + F_{s,n-1}\right)/dt^2, \tag{S35}$$

$$F_{s,n+1} = F_{sum,n+1} - x_{s,n+1}K_{sum,n+1}, \tag{S36}$$

$$F_{s,n} = F_{sum,n} - x_{s,n}K_{sum,n}, \tag{S37}$$

$$F_{s,n-1} = F_{sum,n-1} - x_{s,n-1}K_{sum,n-1}, \tag{S38}$$

Then,

$$x_{s,n+1} = \frac{M_0 + M_1x_n - M_2x_{n-1}}{N}, \tag{S39}$$

$$M_0 = \left(1 + \frac{q_1}{dt} + \frac{2q_2}{dt^2}\right)F_{sum,n+1} - \left(\frac{p_1}{dt} + \frac{2p_2}{dt^2}\right)F_{sum,n} + \frac{p_2}{dt^2}F_{sum,n-1}, \tag{S40}$$

$$M_1 = \frac{q_1}{dt} + \frac{2q_2}{dt^2} + K_{sum,n}\left(\frac{p_1}{dt} + \frac{2p_2}{dt^2}\right), \tag{S41}$$

$$M_2 = \frac{q_2}{dt^2} + K_{sum,n-1}\frac{p_2}{dt^2}, \tag{S42}$$

$$N = \frac{q_1}{dt} + \frac{q_2}{dt^2} + K_{sum,n+1}\left(1 + \frac{p_1}{dt} + \frac{p_2}{dt^2}\right), \tag{S43}$$

$$p_1 = \left(\frac{\eta_1}{E_1} + \frac{\eta_2}{E_1} + \frac{\eta_2}{E_2}\right), p_2 = \frac{\eta_1\eta_2}{E_1E_2}, q_1 = \eta_2, q_2 = \frac{\eta_1\eta_2}{E_1}. \tag{S44}$$

Supplementary Note 5 - Model description: Dynamical equations and the flow chart

➢ *Dynamical equations for intracellular signaling pathways*

The dynamical equations to describe the cytoplasmic signal pathway (***Table S4***) are as follows:

Reaction	Rate	Description
$n_{\text{int}}I_{\text{int}} + N_{FAK}^{ina} \rightarrow n_{\text{int}}I_{\text{int}} + N_{FAK}^{a}$	$r_{1f} = \frac{n_{\text{int}}^2}{n_{\text{int}}^2 + K}[C_{FAK-ina}] + k_{FAK-a}$	n_{int}: the number of active clutch I_{int}: active clutch N_{FAK}^{ina} : inactive FAK N_{FAK}^{a} : active FAK
$N_{FAK}^{a} \rightarrow N_{FAK}^{ina}$	$r_{1r} = k_{FAK-ina}[C_{FAK-a}]$	
$N_{FAK}^{a} + N_{Rho}^{ina} \rightarrow N_{FAK}^{a} + N_{Rho}^{a}$	$r_{2f} = k_{Rho-a}[C_{FAK-a}][C_{RhoA-ina}]$	N_{Rho}^{ina} : inactive Rho N_{Rho}^{a} : active Rho
$N_{Rho}^{a} \rightarrow N_{Rho}^{ina}$	$r_{2r} = k_{Rho-ina}[C_{RhoA-a}]$	
$N_{Rho}^{a} + N_{ROCK}^{ina} \rightarrow N_{Rho}^{a} + N_{ROCK}^{a}$	$r_{3f} = k_{ROCK-a}[C_{ROCK-ina}][C_{RhoA-a}]$	N_{ROCK}^{ina}: inactive ROCK N_{ROCK}^{a}: active ROCK
$N_{ROCK}^{a} \rightarrow N_{ROCK}^{ina}$	$r_{3r} = k_{ROCK-ina}[C_{ROCK-a}]$	
$N_{Rho}^{a} + N_{mDia1}^{ina} \rightarrow N_{Rho}^{a} + N_{mDia1}^{a}$	$r_{4f} = k_{mDia1-a}[C_{mDia1-ina}][C_{RhoA-a}]$	N_{mDia1}^{ina}: inactive mDia1 N_{mDia1}^{a}: active mDia1
$N_{mDia1}^{a} \rightarrow N_{mDia1}^{ina}$	$r_{4r} = k_{mDia1-ina}[C_{mDia1-a}]$	
$N_{ROCK}^{a} + N_{Myosin}^{ina} \rightarrow N_{ROCK}^{a} + N_{Myosin}^{a}$	$r_{5f} = k_{Myosin-a}[C_{Myosin-ina}][C_{ROCK-a}]$	N_{Myosin}^{ina}: inactive myosin N_{Myosin}^{a}: active myosin
$N_{Myosin}^{a} \rightarrow N_{Myosin}^{ina}$	$r_{5r} = k_{Myosin-ina}[C_{Myosin-a}]$	
$N_{mDia1}^{a} + N_{G-actin} \rightarrow N_{mDia1}^{a} + N_{F-actin}$	$r_{6f} = k_{\text{F-actin}}[C_{\text{G-actin}}][C_{mDia1}]$	$N_{G-actin}$: G-actin $N_{F-actin}$: F-actin
$N_{F-actin} \rightarrow N_{G-actin}$	$r_{6r} = k_{\text{G-actin}}[C_{\text{G-actin}}]$	
$N_{YAP/TAZ}^{out} \rightarrow N_{YAP/TAZ}^{in}$	$r_{7f} = k_{YAP-in}[C_{\text{YAP-out}}]$	$N_{YAP/TAZ}^{out}$: cytoplasmic YAP/TAZ $N_{YAP/TAZ}^{in}$: nuclear YAP/TAZ
$N_{YAP/TAZ}^{in} \rightarrow N_{YAP/TAZ}^{out}$	$r_{7r} = k_{YAP-out}[C_{\text{YAP-in}}]$	

where $[C_{\text{molecule}}]$ represents the time-varying amounts of various signaling molecules; $k_{\text{molecule-}a}$ and $k_{\text{molecule-in}a}$ are the activation and deactivation rates of these signals, respectively.

$$\frac{d[C_{FAK-a}]}{dt} = r_{1f} - r_{1r}, \tag{S45}$$

$$\frac{d[C_{RhoA-a}]}{dt} = r_{2f} - r_{2r}, \tag{S46}$$

$$\frac{d[C_{ROCK-a}]}{dt} = r_{3f} - r_{3r}, \tag{S47}$$

$$\frac{d[C_{mDia1-a}]}{dt} = r_{4f} - r_{4r}, \tag{S48}$$

$$\frac{d[C_{Myosin-a}]}{dt} = r_{5f} - r_{5r}, \tag{S49}$$

$$\frac{d[C_{F-actin-a}]}{dt} = r_{6f} - r_{6r}, \tag{S50}$$

where the r_f and r_r are the activation and deactivation rates of signals correspondingly in

Supplementary Note 2.

- *The flow chart of simulation*

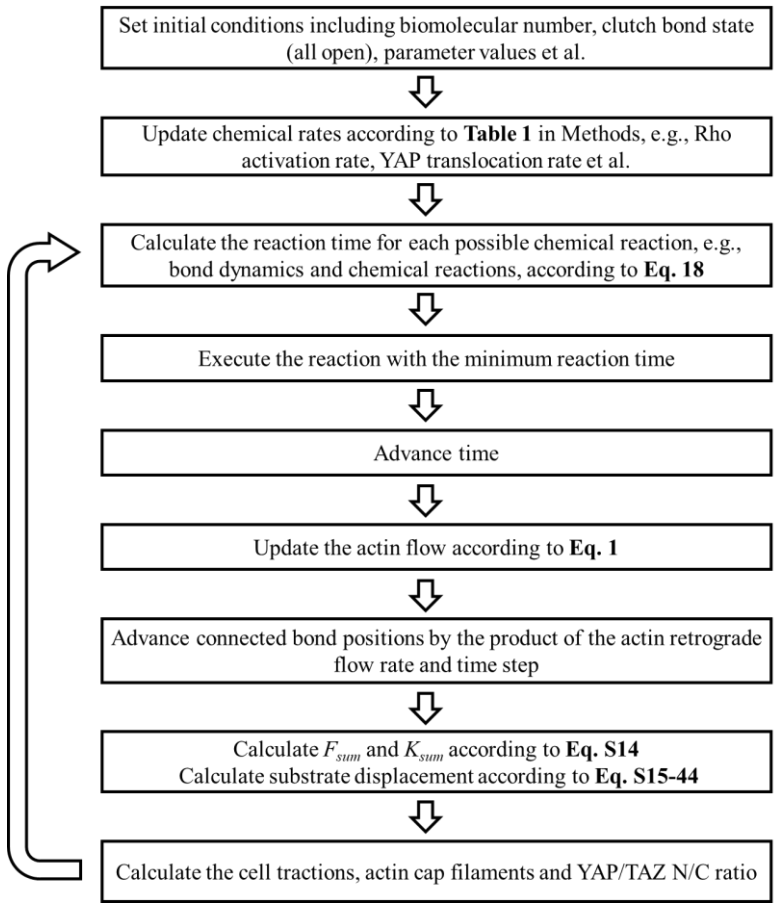

Figure S10. The flow chart for stochastic simulation algorithm.

Supplementary references

1. Molloy, J. E., Burns, J. E., Kendrick-Jones, J., Tregear, R. T. and White, D. C. S. 1995. Movement and force produced by a single myosin head. *Nature*, *378*(6553), 209-212.

2. Bangasser, B. L., Rosenfeld, S. S., and Odde, D. J. 2013. Determinants of maximal force transmission in a motor-clutch model of cell traction in a compliant microenvironment. *Biophys. J.*, *105*(3), 581-592.

3. Chan, C. E., and Odde, D. J. 2008. Traction dynamics of filopodia on compliant substrates. *Science*, *322*(5908), 1687-1691.

4. Elosegui-Artola, A., Bazellières, E., Allen, M. D., Andreu, I., Oria, R., Sunyer, R., ..., Roca-Cusachs, P. 2014. Rigidity sensing and adaptation through regulation of integrin types. *Nat. Mater.*, *13*(6), 631-637.

5. Jiang, G., Giannone, G., Critchley, D. R., Fukumoto, E. and Sheetz, M. P. 2003. Two-piconewton slip bond between fibronectin and the cytoskeleton depends on talin. *Nature*, *424*(6946), 334-337.

6. Litvinov, R. I., Mekler, A., Shuman, H., Bennett, J. S., Barsegov, V. and Weisel, J. W. 2012. Resolving two-dimensional kinetics of the integrin αIIbβ3-fibrinogen interactions using binding-unbinding correlation spectroscopy. *J. Biol. Chem.*, *287*(42), 35275-35285.

7. Lele, T. P., Thodeti, C. K., Pendse, J. and Ingber, D. E. 2008. Investigating complexity of protein–protein interactions in focal adhesions. *Biochem. Biophy. Res. Co.*, *369*(3), 929-934.

8. Roca-Cusachs, P., Iskratsch, T. and Sheetz, M. P. 2012. Finding the weakest link–exploring integrin-mediated mechanical molecular pathways. *J. Cell Sci.*, *125*(13), 3025-3038.

9. Elosegui-Artola, A., Oria, R., Chen, Y., Kosmalska, A., Pérez-González, C., Castro, N., ..., Roca-Cusachs, P. 2016. Mechanical regulation of a molecular clutch defines force transmission and transduction in response to matrix rigidity. *Nat. Cell Biol.*, *18*(5), 540-548.

10. Sun, M., Spill, F. and Zaman, M. H. 2016. A computational model of YAP/TAZ mechanosensing. *Biophys. J.*, *110*(11), 2540-2550.

11. Scott, K. E., Fraley, S. I. and Rangamani, P. 2021. A spatial model of YAP/TAZ signaling reveals how stiffness, dimensionality, and shape contribute to emergent outcomes. *Proc. Natl Acad. Sci. USA*, *118*(20), e2021571118.

12. Asthagiri, A. R., Nelson, C. M., Horwitz, A. F. and Lauffenburger, D. A. 1999.

Quantitative relationship among integrin-ligand binding, adhesion, and signaling via focal adhesion kinase and extracellular signal-regulated kinase 2. *J. Biol. Chem.*, *274*(38), 27119-27127.

13. Sako, Y., Hibino, K., Miyauchi, T., Miyamoto, Y., Ueda, M. and Yanagida, T. 2000. Single-molecule imaging of signaling molecules in living cells. *Single Mol.*, *1*(2), 159-163.

14. Feng, J., Ito, M., Kureishi, Y., Ichikawa, K., Amano, M., Isaka, N., ..., Nakano, T. 1999. Rho-associated kinase of chicken gizzard smooth muscle. *J. Biol. Chem.*, *274*(6), 3744-3752.

15. Ji, H., Tang, H., Lin, H., Mao, J., Gao, L., Liu, J. and Wu, T. 2014. Rho/Rock cross-talks with transforming growth factor-β/Smad pathway participates in lung fibroblast-myofibroblast differentiation. *Biomed. Reports*, *2*(6), 787-792.

16. Cao, L., Kerleau, M., Suzuki, E. L., Wioland, H., Jouet, S., Guichard, B., ..., Jegou, A. 2018. Modulation of formin processivity by profilin and mechanical tension. *Elife*, *7*, e34176.

17. Pollard, T. D. 1986. Rate constants for the reactions of ATP-and ADP-actin with the ends of actin filaments. *J. Cell Biol.*, *103*(6), 2747-2754.

18. Liu, S., Yang, H., Lu, T. J., Genin, G. M. and Xu, F. 2019. Electrostatic switching of nuclear basket conformations provides a potential mechanism for nuclear mechanotransduction. *J. Mech. Phys. Solids*, *133*, 103705.

19. Elosegui-Artola, A., Andreu, I., Beedle, A. E., Lezamiz, A., Uroz, M., Kosmalska, A. J., ..., Roca-Cusachs, P. 2017. Force triggers YAP nuclear entry by regulating transport across nuclear pores. *Cell*, *171*(6), 1397-1410.

20. Bestembayeva, A., Kramer, A., Labokha, A. A., Osmanović, D., Liashkovich, I., Orlova, E. V., ..., Hoogenboom, B. W. 2015. Nanoscale stiffness topography reveals structure and mechanics of the transport barrier in intact nuclear pore complexes. *Nat. Nanotech.*, *10*(1), 60-64.